Optimizing the chemical vapor deposition process of 4H–SiC epitaxial layer growth with machine-learning-assisted multiphysics simulations

Tang, Zhuorui; Zhao, Shibo; Li, Jian; Zuo, Yuanhui; Tian, Jing; Tang, Hongyu; Fan, Jiajie; Zhang, Guoqi

DOI
10.1016/j.csite.2024.104507

Publication date
2024

Document Version
Final published version

Published in
Case Studies in Thermal Engineering

Citation (APA)
Tang, Z., Zhao, S., Li, J., Zuo, Y., Tian, J., Tang, H., Fan, J., & Zhang, G. (2024). Optimizing the chemical vapor deposition process of 4H–SiC epitaxial layer growth with machine-learning-assisted multiphysics simulations. *Case Studies in Thermal Engineering*, *59*, Article 104507. https://doi.org/10.1016/j.csite.2024.104507

Case Studies in Thermal Engineering 59 (2024) 104507

Contents lists available at ScienceDirect

Case Studies in Thermal Engineering

journal homepage: www.elsevier.com/locate/csite

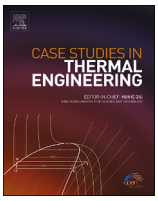

Optimizing the chemical vapor deposition process of 4H–SiC epitaxial layer growth with machine-learning-assisted multiphysics simulations

Zhuorui Tang [a, b], Shibo Zhao [c], Jian Li [d, e], Yuanhui Zuo [f], Jing Tian [a, b], Hongyu Tang [a, b, *], Jiajie Fan [a, b, **], Guoqi Zhang [a, b, g]

[a] Institute of Wide Bandgap Semiconductors and Future Lighting, Academy for Engineering & Technology, Fudan University, Shanghai, 200433, China
[b] Shanghai Research Center for Silicon Carbide Power Devices Engineering & Technology, Fudan University, Shanghai, 200433, China
[c] College of Software, Northeastern University, Shenyang, 110819, China
[d] Technology Innovation Institute of Jilin Province, Changchun, 130000, China
[e] School of AI–Guangdong & Taiwan, Foshan University, Foshan, 528225, China
[f] Research Institute of Fudan University in Ningbo, Ningbo, 315327, China
[g] EEMCS Faculty, Delft University of Technology, 2628, Delft, the Netherlands

ARTICLE INFO

Handling Editor: Huihe Qiu

Keywords:
4H–SiC epitaxial layer
Multi-physical simulation
Machine learning model
CVD
Optimization

ABSTRACT

This work addresses a novel technique for selecting the best process parameters for the 4H–SiC epitaxial layer in a horizontal hot-wall chemical vapor reactor using a transient multi-physical (thermal-fluid-chemical) simulation model and combined with a machine-learning model. An experiment was performed to validate the feasibility of the numerical model. Secondly, a single-factor analysis was conducted to investigate the effects of process parameters, including the deposition temperature, inlet-flow volume, rotational speed of the susceptor, and cavity pressure, on the quality of the 4H–SiC epitaxial layer. Finally, a machine learning algorithm, the ant colony optimization-back propagation neural network (ACO–BPNN), was employed to develop the input/output model and optimize process parameters for obtaining a high-quality epitaxial layer and reducing the optimization cycle and costs. Notably, the optimized process was validated by real experiments, where the error between calculation and experiment is 4.03 % for deposition rate and 0.49 % for coefficient of variation, respectively. The results highlight the model as reliable and lay the foundation for the CVD growth of the 4H–SiC epitaxial layer.

1. Introduction

Wide-bandgap (WBG) semiconductors are considered next-generation semiconductor materials because of their potential in manufacturing electronic and optoelectronic devices. Silicon Carbide (SiC) is a promising material among WBG semiconductors. SiC has a band gap of almost three times that of silicon (Si) and a critical breakdown electric field of 10 times that of Si [1], which can realize the performance of power devices with higher blocking voltage, power, and switching frequency. Furthermore, 4H–SiC exhibits a high saturation electron velocity and thermal conductivity. These characteristics enable the 4H–SiC-based power devices to provide

* Corresponding author. Institute of Wide Bandgap Semiconductors and Future Lighting, Academy for Engineering & Technology, Fudan University, Shanghai, 200433, China.
** Corresponding author. Institute of Wide Bandgap Semiconductors and Future Lighting, Academy for Engineering & Technology, Fudan University, Shanghai, 200433, China.
E-mail addresses: hongyu_tang@fudan.edu.cn (H. Tang), jiajie_fan@fudan.edu.cn (J. Fan).

https://doi.org/10.1016/j.csite.2024.104507
Received 31 January 2024; Received in revised form 26 April 2024; Accepted 7 May 2024
Available online 9 May 2024

considerable advantages over Si-based power devices in high-temperature and high-power areas [2,3]. Several methods were developed for the SiC epitaxial growth, including sublimation, molecular beam epitaxy, and chemical vapor deposition. As proposed by Jokubavicius et al. [4], the growth temperature required by sublimation is the highest, which increases the cost of epitaxial growth. Kitabatake et al. [5] found that molecular beam epitaxy can obtain a high-quality epitaxial layer, but the deposition rate is low. With the emergence of chlorine into the gas mixture [6–8] and the theory of "Step-controlled epitaxy" using off-axis substrates [9,10], chemical vapor deposition (CVD) has become a superior method in 4H–SiC epitaxy compared to others because of the high deposition rate, excellent surface morphology, controllable composition uniformity, and easy mass production.

However, the thickness and uniformity of the 4H–SiC epitaxial layer with CVD growth are affected by many process parameters such as the reactor temperature, cavity pressure, susceptor rotational speed, and flow rate. The conventional process optimizations are mostly based on "trial-error" approaches that require considerable experimentation, which is costly and time-consuming. Therefore, more and more researchers used numerical analysis, i.e. computational fluid dynamics (CFD), to improve the efficiency of their research. Mollick et al. [11] combined CFD with a two-step kinetic mechanism to simulate the deposition rate of SiC on the C/C composite substrate using methytrichlorosilane in a vertical tubular reactor. They revealed that in addition to process parameters such as the flow rate at the inlet and initial wall temperature of the reactor, the sample position and inlet diameter were key parameters for obtaining a high coating rate. Ito et al. [12] studied the effect of wafer rotation and system pressure in the vertical CVD reactor by 2D CFD analysis. The simulation model was consistent with experimental results. They revealed that increasing the rotational speed of the wafer and system pressure was effective in enhancing the epitaxial deposition rate. Nishizawa and Pons [13] combined a 2D CFD model of a horizontal hot-wall reactor (Epigress VP508) with the gas-phase and surface reactions to simulate and study the SiC epitaxial growth and doping in SiH_4, C_3H_8, N_2, and $Al(CH_3)_3$ growth system. They focused on the molar fraction of Si and C under various C/Si ratios and revealed that the site competition due to doping can be calculated by using the C/Si ratio on the growth surface. Dang et al. [14] developed a CFD model of a crucible for top-seeded solution SiC growth to simulate the transport of aluminum, which is crucial for the surface morphology of crystals but easily evaporates. They developed a fin structure in the model to prevent aluminum evaporation and achieved superior surface morphology of crystal experimentally using a fin structure crucible. Deivendran et al. [15] proposed a 3D model for a commercial hot-wall vertical reactor for SiC coating and investigated the effect of various process parameters on flow field stability in a CVD reactor. They determined response surface morphology (RSM) to obtain optimum deposition rate and film uniformity.

Artificial intelligence and machine learning algorithms, including genetic algorithm [16,17], particle swarm optimization [18], neural network [19], and K-nearest neighbor (KNN) [20], becoming increasingly popular, they have been applied in multi-object optimization in engineering to save time and costs. Li et al. [21,22] not only used CFD simulation software to simulate the growth process in the ZnO–MOCVD reaction chamber but also used a neural network model and genetic algorithm to determine the optimal input process parameters for improving film quality. Wang et al. [23] created a surface methodology hybrid with the KNN model to optimize and improve film uniformity by 30 % under a high deposition rate in the plug flow state. Tsunooka et al. [24] used neural network and supported vector regression to develop a rapid prediction of the flow field of CFD simulation for the top-seeded solution growth (TSSG) method in SiC growth. Model prediction of the proposed model was 10^7 times that of CFD simulation only. Isono et al. [25] demonstrated a rapid and precise prediction mode for temperature and fluid flow in the TSSG crucible by changing the structure and process parameters using a neural network. They used a genetic algorithm to determine the optimal variable parameters for the 6-inch TSSG condition. To date, limited studies have been conducted on 3D modeling and optimization of process parameters to improve the quality of 4H–SiC epitaxial growth in the commercial horizontal hot-wall reactor based on TCS and C_2H_4 growth system.

In this study, we simulated the 4H–SiC epitaxial growth process through CFD calculations coupled with the thermal-fluid-chemical multi-physical model, and we compared the deposition rate of simulation with the experimental results to confirm the reliability of the numerical model. Single parameter analysis was conducted through simulation on the process parameters that affect the deposition rate and uniformity of 4H–SiC epitaxial growth. These parameters included the inlet-flow volume, rotational speed of susceptor, growth temperature, and cavity pressure. The relationship between the combination of process parameters and film quality was developed through a back propagation neural network (BPNN) to predict the epitaxial uniformity and deposition rate within the allowable range. Further, optimization was performed on the ant colony algorithm. This study indicated the direction for 4H–SiC epitaxial growth process debugging.

2. Models and process condition

2.1. Apparatus

In this study, an industrialized hot-wall horizontal "Epi-150" 4H–SiC epitaxial CVD equipment was used, as shown in Fig. 1(a). The system mainly consisted of six subsystems, namely the reaction chamber system, gas-delivering system, load-lock system for wafer transfer, software and hardware control system, vacuum system, and heating system. The reaction chamber was placed horizontally, and the outermost layer of the reaction chamber was surrounded by an induction heating coil and a translucent quartz tube. The induction coil and quartz tube are hollow in the middle, which is filled with deionized water as a coolant, as shown in Fig. 1 (b).

Fig. 1 (c) shows the structural front view of the CVD reactor in which the down and up crucible consists of dense graphite, and semicircular shaped hollow inside crucibles are designed to create an eddy current to heat the 4H–SiC wafer in the middle of the cavity. Furthermore, two graphite crucibles are wrapped with graphite felt for thermal insulation. Fig. 1 (d) shows a part of the gas-delivering system. Here, C_2H_4 as a C source gas and TCS as a Si source gas are partially mixed with purified carrier gas H_2 in three gas transportation pipelines before introduction into the cavity. Three needle valves at upstream of the cavity were used to control these three gas flow volumes.

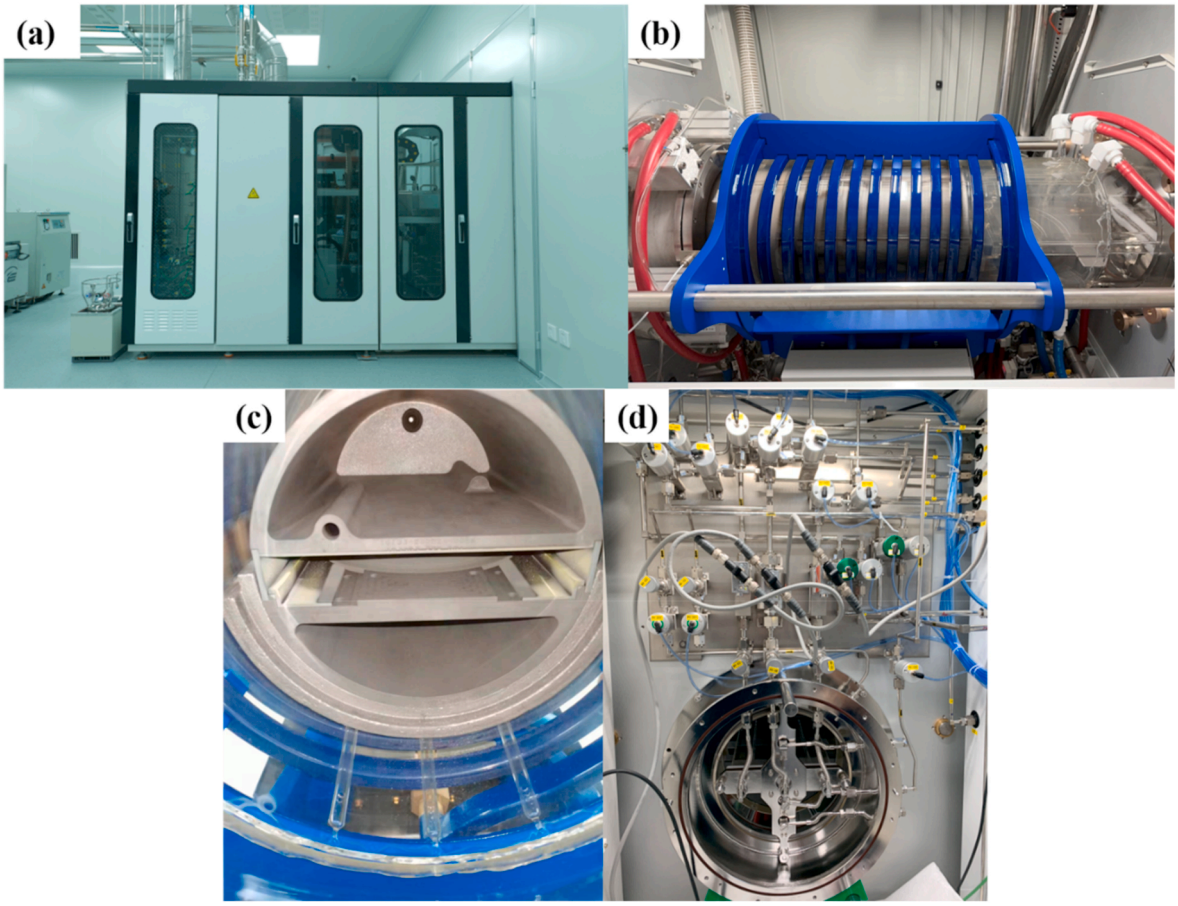

Fig. 1. Hot-wall horizontal 4H–SiC epitaxial growth system: (a) Appearance of whole equipment. (b) Reaction chamber and heating system. (c) Front view of reaction cavity. (d) Part of the gas-delivering system.

2.2. Standard condition, numerical model, and characterization

Fig. 2(a) shows the structure diagram of the whole reaction chamber. Here, H_2 carried the reaction gas (TCS and C_2H_4) through three gas flow tunnels, whose objective was to uniformly mix the flow before entering the cavity. The substrate was placed at the center of the gas-foiled rotational susceptor. The substrate was spun with the susceptor during the growth process. The flow volume of flotation gas, which has a pipeline beneath the susceptor, adjusted the rotating speed. The exhaust vent was connected with a butterfly valve downstream of the cavity to control the reaction chamber pressure. Fig. 2 (b) shows the schematic diagram of deposition under standard operating conditions. The flow rate of the inlet gas includes the carrier gas (H_2) and reaction gas (C_2H_4, TCS). The sum of H_2, C_2H_4, and TCS at the chamber inlet was $Q = 100$ slm. Among them, the ratio of the Si source (TCS) and C source (C_2H_4) was fixed at 1.3. The ratio of the inlet-flow volume was 1:2:1 at the left side, middle, and the right-side spray tunnel, respectively. The rotational speed of the susceptor inside the cavity was 60 rpm, and the pressure of the cavity was set to 100 mbar.

In the experiment, the thickness was measured by using Fourier transform infrared spectroscopy (Nicolet iS50). The root mean square (RMS) of roughness values was determined and surface morphology was observed using Bruker Dimension Icon atomic force microscope system. The crystallinity and element content were characterized by high resolution X-ray diffraction systems (XRD, Bruker AXS) using Cu Kα radiation (40 kV, 40 mA, $\lambda = 1.54$ Å) and energy dispersive X-Ray spectra (EDS) function in double beam electron microscopy (Helios 5 Hydra CX), respectively.

2.3. Governing equations and chemical reaction kinetics in the multi-physics simulations

SiC epitaxial growth is complex and relates to the temperature filed, flow field, chemical reaction, etc. Thus, a multi-physics simulation coupled the thermal-fluid-chemical model was performed with the following equations: continuity, momentum, energy, and species transport. Here, SiC epitaxial layer grow in a low-pressure and laminar flow state environment. In this condition, the reaction gas was subsonic and incompressible.

The continuity equation is as follows:

$$\nabla \bullet \left(\rho \vec{v}\right) = 0 \tag{1}$$

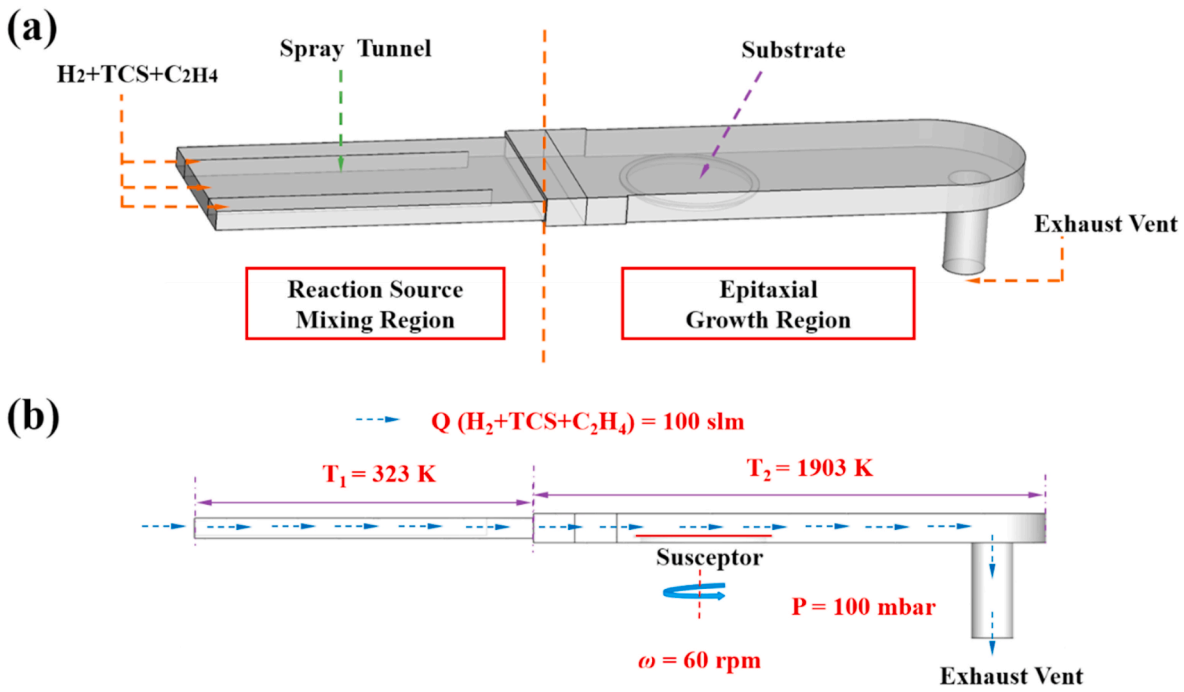

Fig. 2. SiC epitaxial reaction cavity of (a) structure diagram and (b) schematic diagram of deposition under standard operating conditions.

where ρ is the mass density, and $\vec{v}$ is the gas mixture velocity.

The momentum balance equation is as follows:

$$\nabla \bullet \left(\rho \vec{v} \bullet \vec{v}\right) = \nabla \overline{\overline{\tau}} - \nabla p + \rho \vec{g} \tag{2}$$

where p is the pressure inside the cavity, $\vec{g}$ represents the gravitational acceleration, and $\overline{\overline{\tau}}$ is the sheer stress tensor, which is given by

$$\overline{\overline{\tau}} = \mu\left(\nabla \vec{v} + \left(\nabla \vec{v}\right)^{T}\right) - \frac{2}{3}\mu\left(\nabla \vec{v}\right) \bullet I \tag{3}$$

where μ is the dynamic viscosity, and I is the unit tensor.

The energy balance equation is expressed as follows:

$$C_p \nabla \bullet \left(\rho \vec{v} T\right) = \nabla \bullet (k \nabla T) + \sum_{i=1}^{N} \frac{H_i}{M_i} \nabla \bullet \vec{J_i} - \sum_{i=1}^{N} \frac{H_{i,0}}{M_i} R_i \tag{4}$$

where C_p is the specific heat capacity, k is the thermal conductivity, and T is the temperature in the cavity. Here, H_i, M_i, J_i, and $H_{i,0}$ represent molar enthalpy, molar mass, diffusion flux of mass, and enthalpy of formation, respectively. In Eq. (4), the expression on the left describes heat transfer due to convection, whereas the three expressions on the right represent heat conduction, species diffusion, and chemical reactions. Here, R_i is the net volumetric rate of the ith component in the chemical reaction.

$$R_i = M_i \sum_{i=1}^{K} v_{ik} \left(\hat{R}_k^i\right) \tag{5}$$

Species transport equation can be expressed as follows:

$$\nabla \bullet \left(\rho \vec{v} w_i\right) = -\nabla \bullet \vec{J_i} + M_i \sum_{j=1}^{K} R_j^i \tag{6}$$

where w_i is the mass fraction of the ith component, and R_j^i is the net volumetric rate of i species produced in reaction j. According to Maxwell–Stefan theory, the diffusive flux $\vec{J_i}$ includes diffusive flux due to the concentration gradient and diffusive flux driven by the temperature. This phenomenon can be represented as follows:

$$\overrightarrow{J_i} = -\sum_{j=1}^{N} \rho D_{i,j} \nabla w_i - D_i^T \frac{\nabla T}{T} \tag{7}$$

where $D_{i,j}$ and D_i^T are the multicomponent diffusion coefficient matrix and multicomponent thermal diffusion coefficient matrix, respectively.

The density of a gas mixture is defined as follows:

$$\rho = \frac{P_{op} \mathrm{M_w}}{\mathrm{R}T} \tag{8}$$

where P_{op}, $\mathrm{M_w}$, and R are the pressure inside the reaction cavity, the molecular weight of the gas, and the universal gas constant, respectively.

The numerical simulation of the CVD reactor of 4H–SiC in the $SiHCl_3/C_2H_4/H_2$ system was described by four chemical reactions, including three gas phase reactions and one surface reaction. These equations were obtained from the literature [26–28] as shown in the following:

Gas-phase reactions:

$$SiHCl_3 \rightarrow SiCl_2 + HCl \tag{9}$$

$$C_2H_4 \rightarrow C_2H_2 + H_2 \tag{10}$$

$$6SiCl_2 + 3C_2H_2 + 3H_2 \rightarrow 6SiC + 12HCl \tag{11}$$

The surface reaction is as follows:

$$2SiCl_2 + C_2H_2 + H_2 \rightarrow 2SiC + 4HCl \tag{12}$$

2.4. Mesh description and boundary conditions

To control the mesh quality (Fig. 3), a hexahedral mesh was designed in ICEM software. The number of grids was 1 million. CFD simulation was conducted by the commercial software FLUENT 14.0 with a pressure-based solver. SIMPLEC was used for the pressure and velocity-coupling algorithm, and second-order upwind spatial discretization was used for the momentum, component, and energy equations. The standard scheme was used for pressure interpolation. The residual convergence criterion was 1E−6 for the energy equation and 1E−4 for the other equations. Numerical calculation was performed on HPZ820 work-stations (dual Intel Xeon E5-2690/128G DDR3 memory/NVIDIA Quadro 5000). The time for computing a single case was approximately 2 h.

Moreover, the following assumptions and boundary conditions were set to solve the mathematical model of the system.

1. The growth of materials was stable and the flow field was laminar because the Reynolds number was <2300.
2. The inner wall was assumed to be nonadiabatic, and the inlet wall and flow rate was set to 323 K.
3. The dense graphite exhibits excellent thermal conductivity, and the epitaxial growth region temperature was 1903 K, which is identical to that of the substrate.

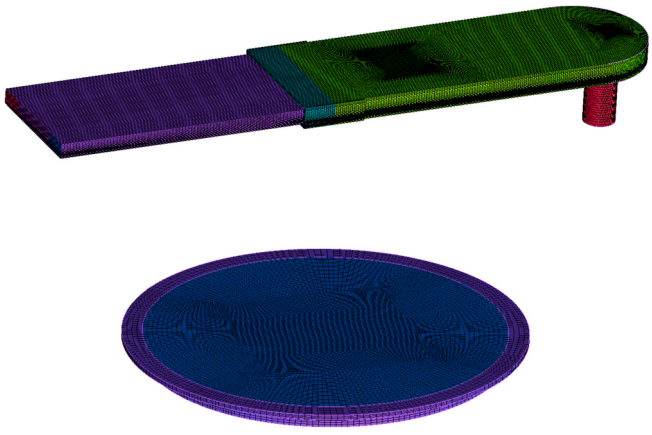

Fig. 3. Mesh model diagram of the SiC reactor.

3. Results and discussion

3.1. Multi-physics model validation and analysis under the standard condition

The substrates in the model were 6 inches in diameter. Seven sampling points, as shown in Fig. 4(a), were set to monitor the film's thickness and uniformity, which were measured and calculated using the average deposition rate and coefficient of variation, as expressed in Eq. (13) and Eq. (14), respectively.

$$\bar{x} = \frac{\sum_{i=1}^{n} x_i \times S_i}{S} \tag{13}$$

$$C_v = \frac{\sqrt{\frac{1}{n-1}\sum_{i=1}^{n}\left(x_i - \bar{x}\right)^2}}{\bar{x}} \tag{14}$$

where x_i and $\bar{x}$ are the radial deposition rate in region i and the average deposition rate, respectively. Here, S_i and S are the area of region i and the area of the growth region, respectively. A higher average deposition rate indicates a greater thickness, and a larger coefficient of variation indicates inferior uniformity.

Fig. 4 (b) shows a comparison between the experimental and simulation results of seven monitoring points on the 6-inch 4H–SiC epitaxial layer under standard operating conditions. The simulation results were consistent with the experimental results. The overall average error of the deposition rate between numerical simulation (55.90 μm/h) and experiment (57.57 μm/h) was 2.88 %. The maximum and minimum errors among these monitoring points were 4.57 % and −0.81 %, respectively. Furthermore, the coefficient of variation of the experiment was 4.24 % and that of the numerical simulation was 5.89 %. Therefore, the simulation model was feasible and accurate, which could be used for the optimization of process parameters.

Fig. 5 (a) reveals that the inlet-flow into the reaction chamber was categorized into three spray tunnels. The streamline was smooth and no vortices were generated inside the ~~cavity~~ reaction chamber. In this structure and condition, the flow was stable and suitable for material growth. Fig. 5 (b) shows the temperature distribution in the simulation. Since the reactant flows towards the exhaust vent, the temperature the downstream of reactor chamber has a slight influence on the upstream deposition rate of the susceptor area. To simplify the simulation process and reduce the simulation time, the temperature of the whole reaction chamber was originally set the same such as 1903 K under standard conditions, which is not the case in reality. In the simulation, the influence of the inlet flow on the temperature occurred in the spray tunnel, and the temperature remained the same as the pre-set 1903K. Under this flow rate, the temperature of the deposition core area was not affected.

3.2. Influence of process parameters on thin-film property

Several process parameters, such as inlet-flow volume, rotational speed of susceptor, cavity pressure, and temperature, affect the properties of the epitaxial SiC film. In the epitaxial growth process, the higher deposition rate contributed to the production efficiency and reduction of defects [29–32]. The higher uniformity directly affects the film quality as well as the subsequent yield of power de-

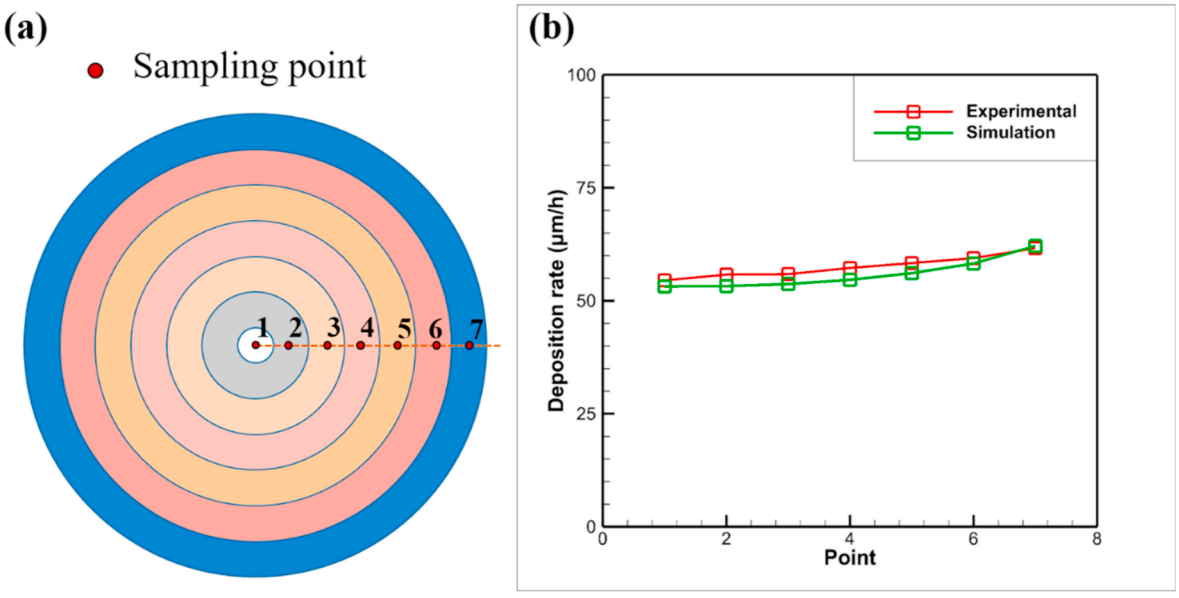

Fig. 4. (a) Monitoring points for 6-inch SiC epitaxial wafers. (b) Comparison of experimental and simulated SiC film deposition rates under the standard process condition.

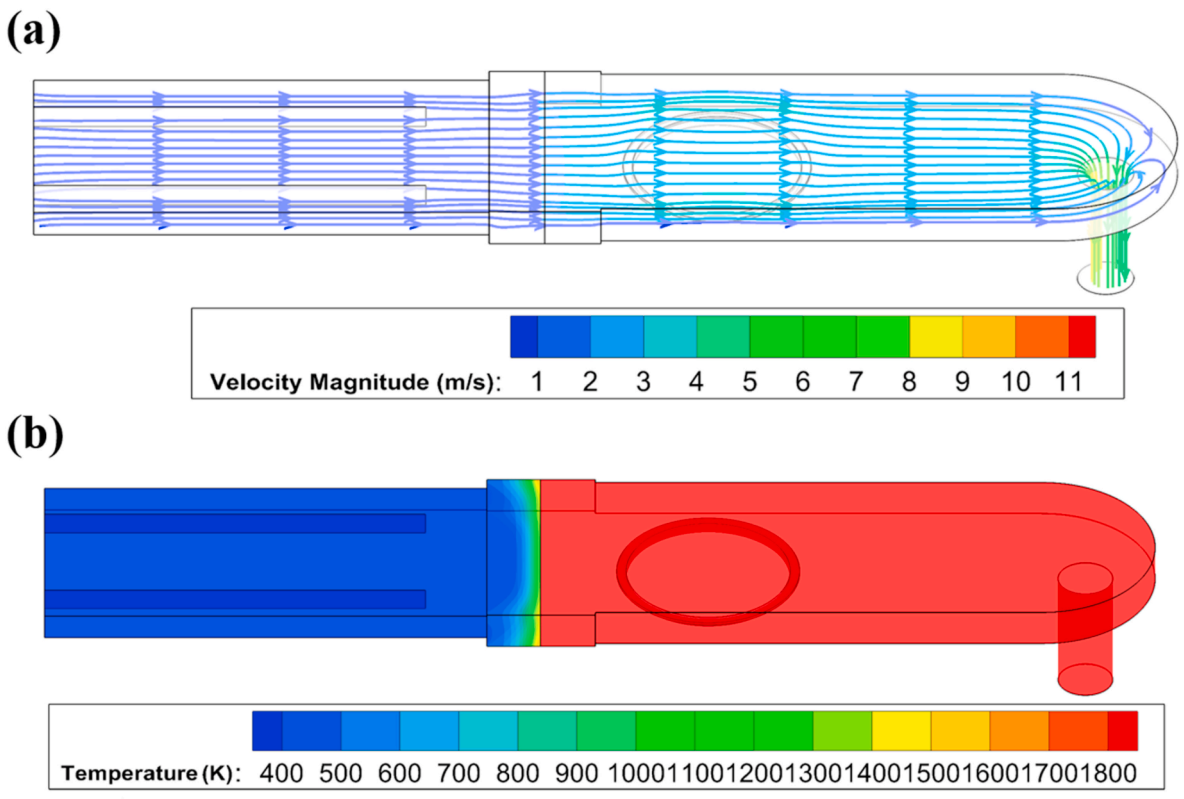

Fig. 5. SiC epitaxial reaction chamber under standard condition of (a) velocity streamline and (b) temperature distribution.

vices [33].To analyze the effects of these parameters on the deposition rate and uniformity of SiC thin film, we changed one factor at one time as presented in Table 1, and the other parameters were consistent with the standard operating condition.

3.2.1. *Effect of inlet-flow volume*

The volume of carrier and reaction gases plays a crucial role in CVD 4H–SiC epitaxial growth. The inlet-flow volume (the sum of carrier gas and reaction gas) affects the transport and diffusion rate of reaction gases, the distribution of the reactant in the cavity, and the deposition rate and uniformity of the thin film. Fig. 6 (a) shows the deposition map of seven monitoring points. Fig. 6 (b) shows the average deposition rate and coefficient of variation under various inlet-flow volumes. With the increase in the inlet-flow volume, the average deposition rate of the thin film gradually increased. The increase in the inlet-flow volume accelerated the decomposition and reaction rate of the reactant. By contrast, the coefficient of variation gradually decreased as the inlet-flow volume increased, which improved the uniformity of the thin film and achieved superior quality of the film growth. The larger the inlet-flow volume was, the faster the transportation and diffusion rate of the reaction gas were, and the more uniform the distribution of the reaction gas in the reaction chamber was. The pre-reaction of the reactant was also reduced. Thus, film uniformity was better with increase of inlet-flow volume.

3.2.2. *Effect of cavity pressure*

Fig. 7 (a) and (b) show the deposition rate of seven monitoring points, the average deposition rate, and the coefficient of variation at various pressures of the cavity. As the pressure increased, the deposition rate of the thin film increased first. However, when the cavity pressure surpassed 100 mbar, the deposition rate decreased with the increase in pressure. The coefficient of variation increased with the increase in pressure. With the increase in pressure, the molecular density of the reactant gradually increased, but the flow speed in the cavity gradually decreased. Molecular density had a significant effect on the deposition rate when the pressure was less than 100 mbar. By contrast, the influence of the slow flow speed exceeded that of the molecular density and became a primary

Table 1
Parameters of single-factor analysis.

Process Parameters	Values				
Q (slm)	25	50	100	125	150
P (mbar)	75	100	125	150	175
ω (rpm)	0	25	50	75	100
Temperature (K)	1843	1873	1903	1943	1973

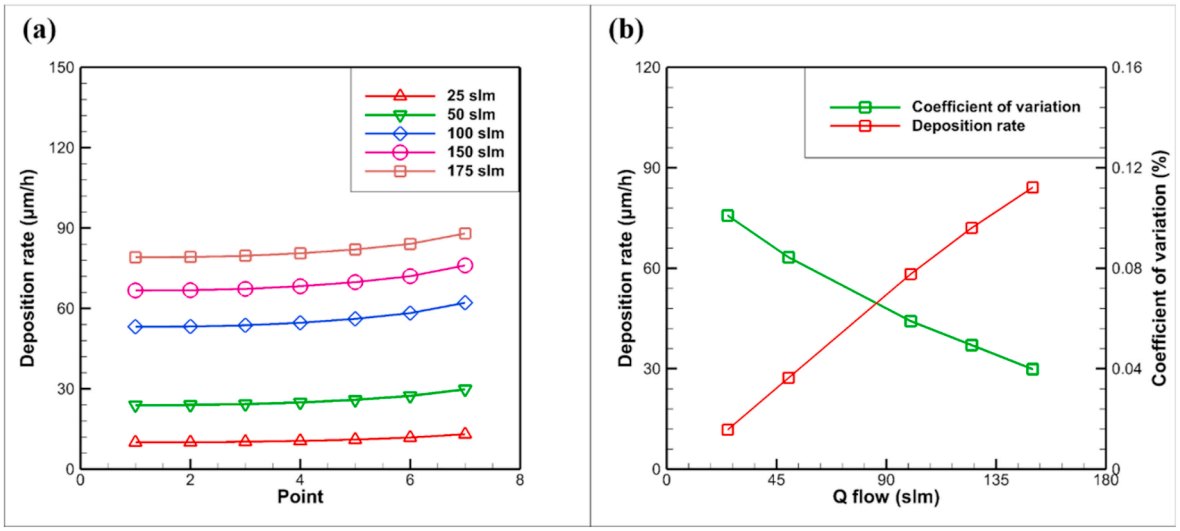

Fig. 6. SiC epitaxial growth under various inlet-flow volumes. (a) Seven points distribution maps. (b) Average deposition rates and coefficient of variations.

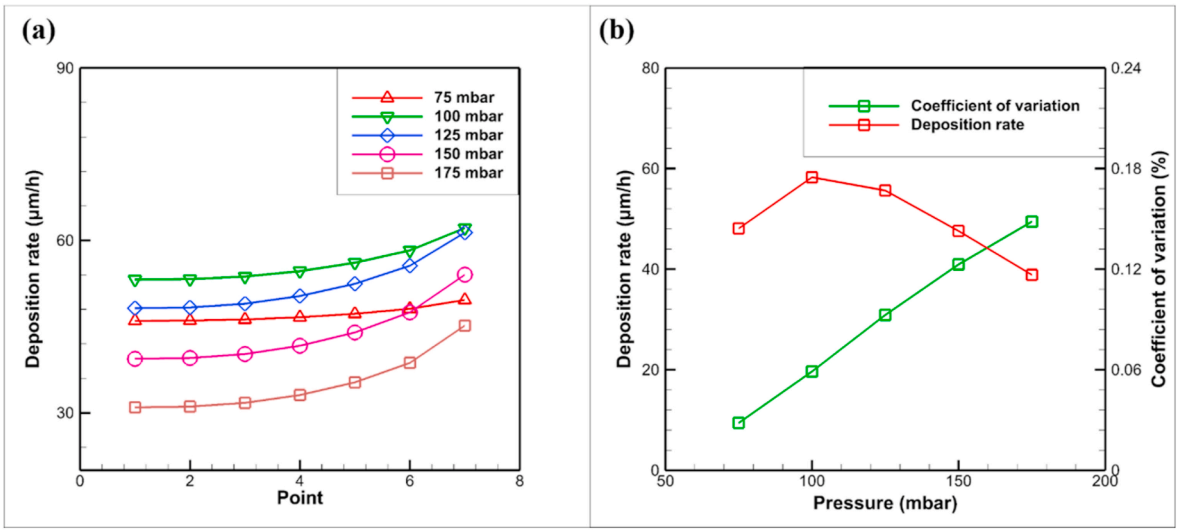

Fig. 7. SiC epitaxial growth at various pressures. (a) Seven-point distribution maps. (b) Average deposition rates and coefficient of variations.

factor with a consistent increase in pressure. Flow speed gradually conduced to decrease transport and diffusion rate of the reactant, which reduced the deposition rate and uniformity of thin-film growth. Furthermore, the "boundary layer theory" proposed by Ref. [34], i.e., the greater the pressure, the thicker the boundary layer, can explain the tendency of the deposition rate. When the pressure was lower than the critical value, the higher flow speed carried the reactant get through the boundary layer and deposited it on the substrate. However, when the pressure exceeded the critical value, the slower flow speed rendered carrying the atoms of reactant diffusion to the substrate difficult. Thus, this resulted in a decrease of the deposition rate to a large extent.

3.2.3. Effect of the rotational speed of susceptor

During SiC epitaxial growth, the susceptor, which carries the substrate, was given a certain rotational speed to promote the uniform distribution of the reactant on the surface of the substrate. Fig. 8(a) and (b) show the distribution trend of deposition rate at seven monitoring points, as well as the average deposition rate and coefficient of variation at various rotational speeds. Comparing the stationary and rotational susceptors, the stationary susceptor exhibits a high coefficient of variation and poor uniformity. For the rotational susceptor, the deposition rate of seven monitoring points tended to be consistent at various rotational speeds. The average deposition rate was greater than the condition of the stationary susceptor. Furthermore, the coefficient of variation of the rotational susceptor decreased sharply. Thus, a significant improvement occurred in the uniformity of the thin film. The rotational speed of the susceptor positively affect the deposition rate and thin film uniformity.

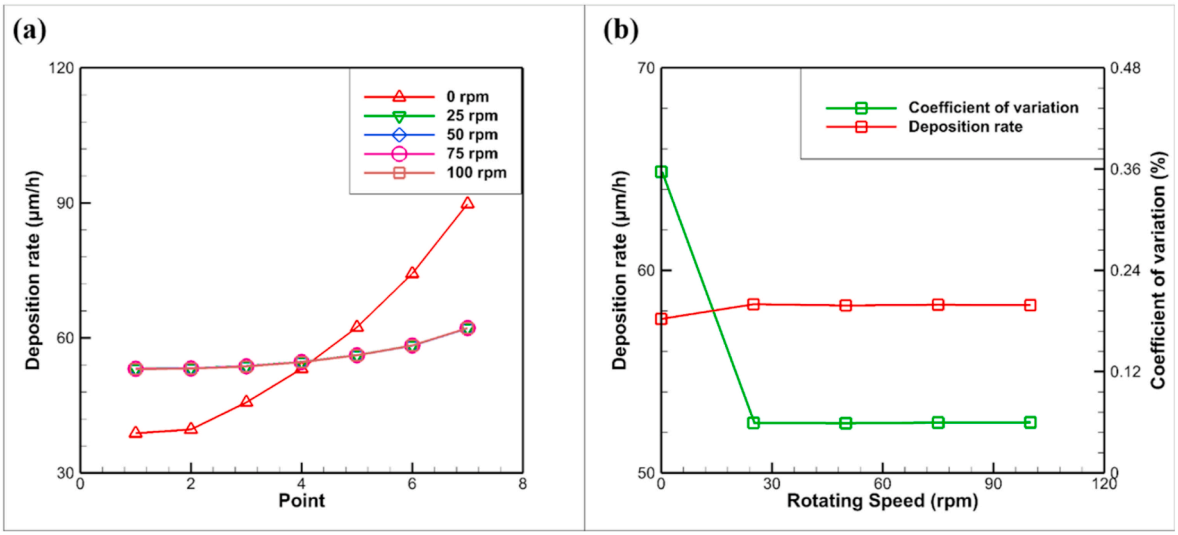

Fig. 8. SiC epitaxial growth at various rotational speeds. (a) Seven-point distribution maps. (b) Average deposition rates and coefficient of variations.

3.2.4. Effect of the growth temperature

SiC epitaxial growth should be performed in a high-temperature environment, and the temperature considerably affects the quality of thin-film deposition. Fig. 9(a) shows the distribution trend of deposition rate at seven monitoring points. The deposition rate in the middle of the wafer was slow, but it became fast at the edge of the wafer. Fig. 9 (b) shows the average deposition rate and coefficient of change under various temperatures. With the increase in temperature, the deposition rate of the thin film gradually decreased and the coefficient of variation increased because the increase in temperature resulted in the decomposition of the reaction gas, resulting in uneven gas mixing or parasitic reactions in the reaction chamber, which affects the composition of 4H–SiC and subsequently affects the thickness uniformity and deposition rate of the film.

4. Optimization of process parameters based on the ACO-BPNN

In the 4H–SiC CVD system, the thermal and flow fields interact with each other, resulting in various combinations of multiple process parameters that are not linear in their effect on the film deposition rate and uniformity. Figuring out this nonlinearity and determining optimal process parameters based on actual growth experiments are time consuming and cumbersome. The BPNN and ACO combined with numerical simulation are applicable and cost-saving methods to develop the nonlinear model on input/output and to determine the optimal combination of process parameters. From the results of the single-factor analysis, except for the various rotational speeds of the susceptor, the inlet-flow volumes, cavity pressure, and growth temperature have huge impact on the quality of the 4H–SiC epitaxial layer. In such a case, the rotational speed of the susceptor was the same as the standard condition at 60 rpm, and

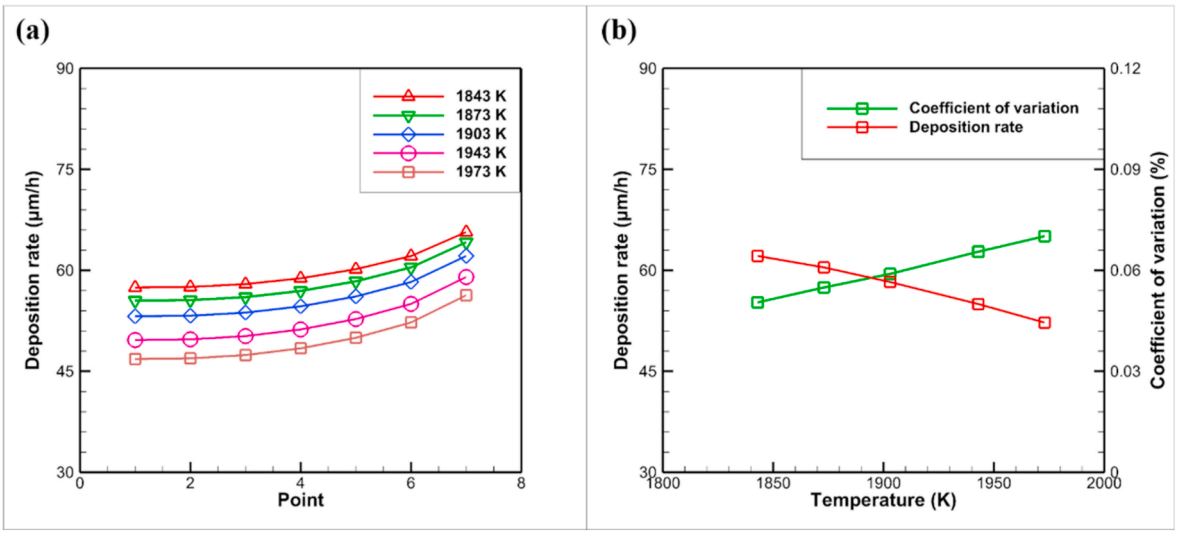

Fig. 9. SiC epitaxial growth at various growth temperatures. (a) Seven point distribution maps. (b) Average deposition rates and coefficient of variations.

three other process parameters were picked for a subsequent input of ant colony optimization-BPNN (ACO–BPNN) algorithm to determine the optimal thin-film uniformity and deposition rate.

4.1. Optimization procedure

As shown in Fig. 10, the operation of ACO–BPNN is detailed as follows:

We randomly generated 60 groups with a combination of process parameters including 50 groups as the training set of the neural network and the remaining 10 groups as the validation set for the BPNN model verification. As shown in Fig. 11, the NN had three layers: an input layer (inlet-flow volume, cavity pressure, and growth temperature), an output layer (deposition rate and coefficient of variation), and a hidden layer. Table 2 presents the range of these process parameters. Table S1 presents these 50 groups' experiments and their corresponding epitaxial deposition rate and coefficient of variation by calculating the deposition rate at seven monitoring points. Table S2 presents a comparison of the BPNN prediction and numerical simulation results. The errors were <1 %, which implied that the BPNN had high prediction accuracy.

After BPNN training and error calculation based on the dataset, the ACO was used, and the BPNN model was integrated into the ant colony algorithm for the optimization of multiple process parameters. The steps for ACO are as follows.

(1) Initialization of algorithm parameters: set the number of ants m in the ant colony algorithm to 20; the maximum number of iterations was 400; the pheromone evaporation coefficient R_{ho} was 0.9; the transfer probability constant was set to 0.2; the local searching step size was set to 0.1; to increase the convergence speed, the importance factor of pheromone α was set to 1 and that of heuristic function β was set to 8.

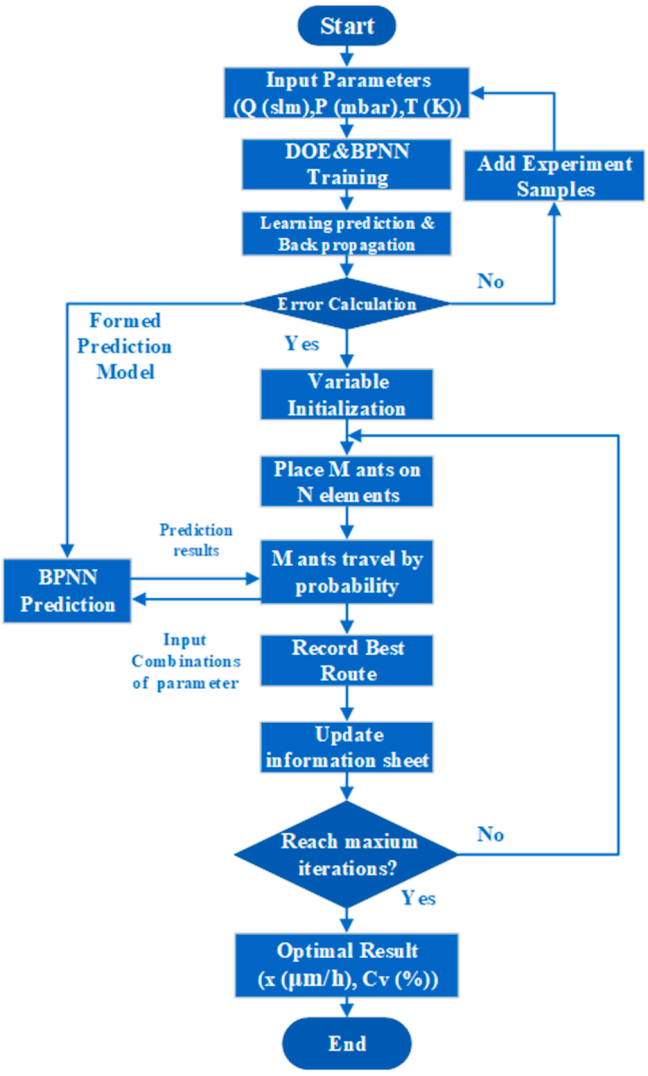

Fig. 10. Flowchart of the ACO–BPNN.

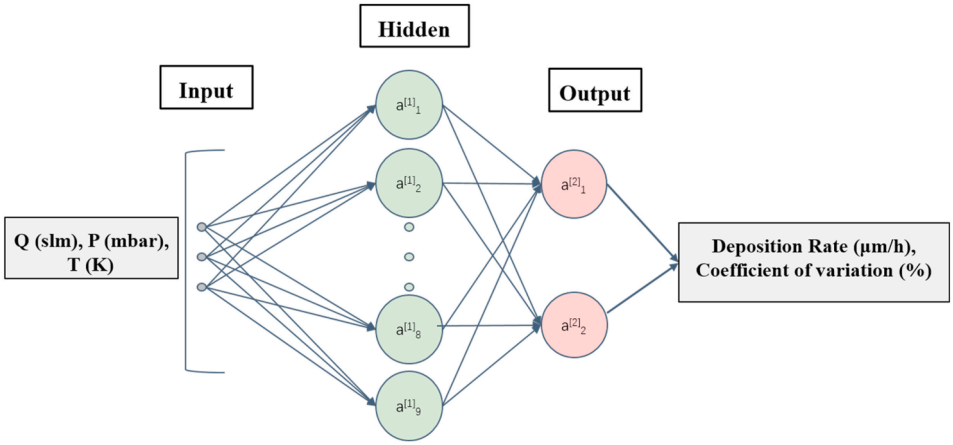

Fig. 11. Neural network topology diagram.

Table 2
Range of processing parameters for the ant colony optimization-back propagation neural network (ACO–BPNN).

Parameters		Inlet-flow volume (slm)	Pressure (mbar)	Temperature (K)
Input	Lower bound	50	75	1873
	Upper bound	150	150	1943
Output	Deposition rate (μm/h) and coefficient of variation (%)			

(2) Generate ant positions randomly, and subsequently, generate initial pheromone paths according to the neural network. Calculate the probability of state transfer.
(3) Perform local search when the state transfer probability is less than the transfer probability constant. After local search, perform a global search to generate new ant positions. The boundary absorption method is adopted to deal with the boundary conditions.
(4) Recalculate the fitness to determine whether the ant has moved. If the ant has moved, then the pheromone path is updated using the BPNN.
(5) Check whether the termination condition is satisfied; if so, terminate the procedure to output the optimized value; otherwise, return to process (2) to continue the iteration.

4.2. Results of optimization

As shown in Fig. 12, after 200 iterations using the ant colony algorithm, fitness became stable, and the path with the most pheromones was identified. The optimal combination of process parameters for both deposition rate and coefficient of variation was determined after ACO-BPNN.

The deposition rate and coefficient of variation results of the standard condition, simulated optimized combination of the process parameter, and the results of the experiment are presented in Table 3. The optimal combination of process parameters after ACO-BPNN was 135.28 slm, 1887.2 K, and 81.4 mbar. The corresponding deposition rate and coefficient of variation were 69.526 μm/h and 2.04 %, respectively. Compared with the standard conditions, the optimized results enhanced the deposition rate by 17.2 % and the coefficient of variation by 51.88 %.

To investigate the film quality and ensure the correctness of ACO-BPNN results, an experiment was conducted after ACO-BPNN. The error between prediction results of ACO-BPNN and real experiments under the prediction condition was 4.03 % for the deposition rate and 0.49 % for the coefficient of variation. The thickness distribution for experiments under ACO-BPNN conditions and standard conditions can be seen in Fig. 13(a). It shows an enormous improvement in thin-film growth efficiency and uniformity. The epitaxial wafer that grows under ACO-BPNN condition can be seen in Fig. 13(b). Furthermore, 9 scanning points for surface morphology and roughness characterization can be also seen in Fig. 13(b). The corresponding 2D and 3D surface morphology images of L-1, Center, R-1, U-1, and D-1 are shown in Fig. 14. Fig. S1 displays the other surface morphology images of L-2, R-2, U-2, and D-2. Under the optimized combination of the process parameter, the average surface RMS value (R_a) for these 9 points was 0.177 nm, which indicates that the epitaxial surface was smooth.

Fig. 15(a) depicts the rocking curve spectra of 5 scanning points, which are measured with typical XRD spectra of a 4H–SiC single crystal whose medium incident angle is around 21.7° [35]. The average full width at half maximum (FWHM) of this peak is 19.19 arcsec. Fig. 15(b) demonstrates a dimension of 5 μm ×5 μm EDS pattern at the epitaxial wafer center. The result showed that only Si and C were found. They accounted for 54.22 % and 45.78 %. It implies that the Si atom and the C atom successfully intertwine to form SiC epitaxial layer. All these characterization results denote that the epitaxial wafer satisfies the requirement for the subsequent production of power devices. Additionally, the uniformity of doping concentration and defect distribution are also important for the quality of SiC epitaxial layer, which will be studied by using multi-scale simulations and experiments in our future works.

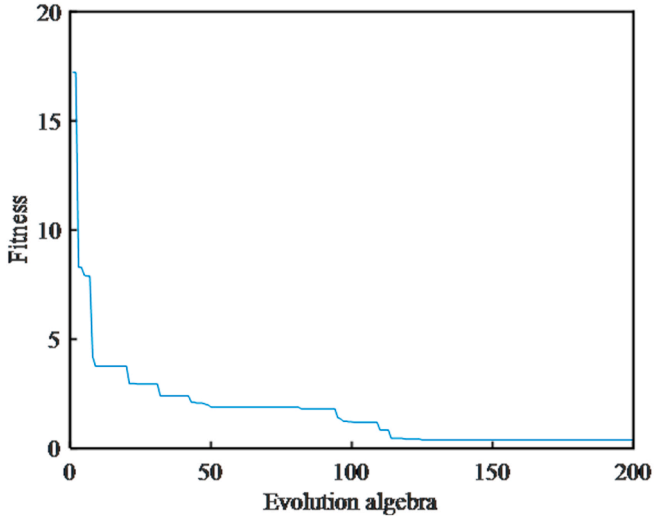

Fig. 12. Fitness evolution curve.

Table 3
Comparison of the standard condition and optimal combination of the process parameter after ACO-BPNN.

Condition	Inlet-flow Volume (slm)	Growth Temperature (K)	Cavity Pressure (mbar)	Deposition Rate (μm/h)	Coefficient of Variation (%)
Standard Condition	100	1903	100	57.57	4.24
Optimized (Calculation)	135.28	1887.2	81.4	69.53	2.04
Optimized (Experiment)	135.28	1887.2	81.4	72.45	2.05
Improvement of Deposition Rate: 17.2 % and Coefficient of Variation: 51.88 %.					
Error between calculation and experiment after optimized with ACO-BPNN: 4.03 % for deposition rate and 0.49 % for coefficient of variation.					

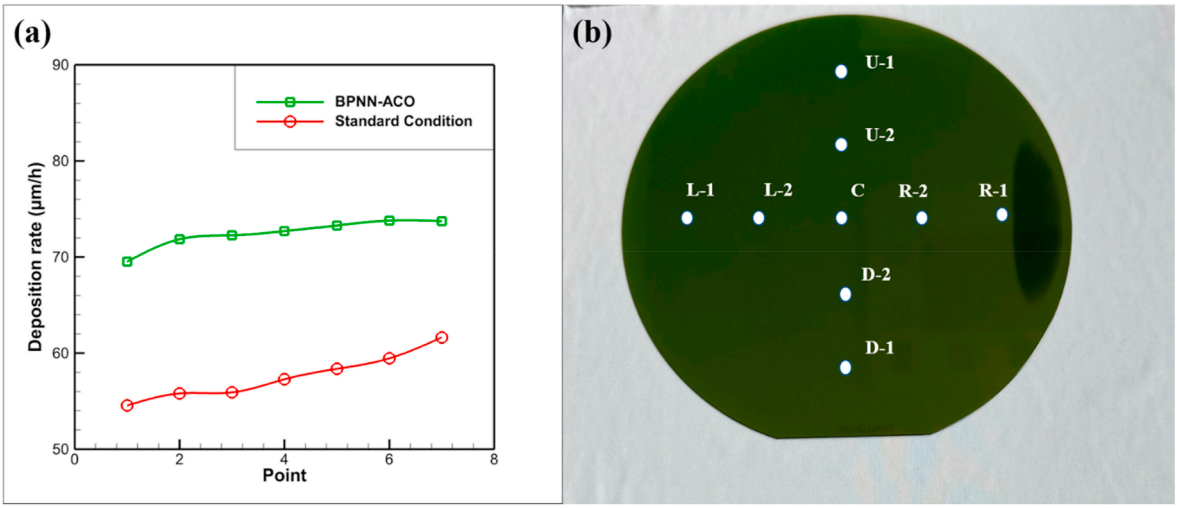

Fig. 13. (a) Thickness distribution of experiment under ACO-BPNN condition and standard condition. (b) 4H–SiC epitaxial wafer and characterization points.

5. Conclusion

In this study, the 4H–SiC epitaxial growth numerical simulation of horizontal hot-wall "Epi-150" 4H–SiC CVD reactor was established by the thermal-fluid-chemical multi-physics model. The influence of process parameters including inlet-flow volume, cavity pressure, growth temperature, and rotational speed of the susceptor on the film quality was studied. Prediction and optimization between the combination of multiple process parameters and film quality were carried out by using the ACO–BPNN method. The conclusions are as follows.

(1) Under standard operating conditions, the deposition rate and coefficient of variation errors between numerical simulation and experiment were 2.88 % and 1.65 %, respectively. This proved the feasibility of numerical simulation, and it can be used for further optimization on both reactor design and growth process.

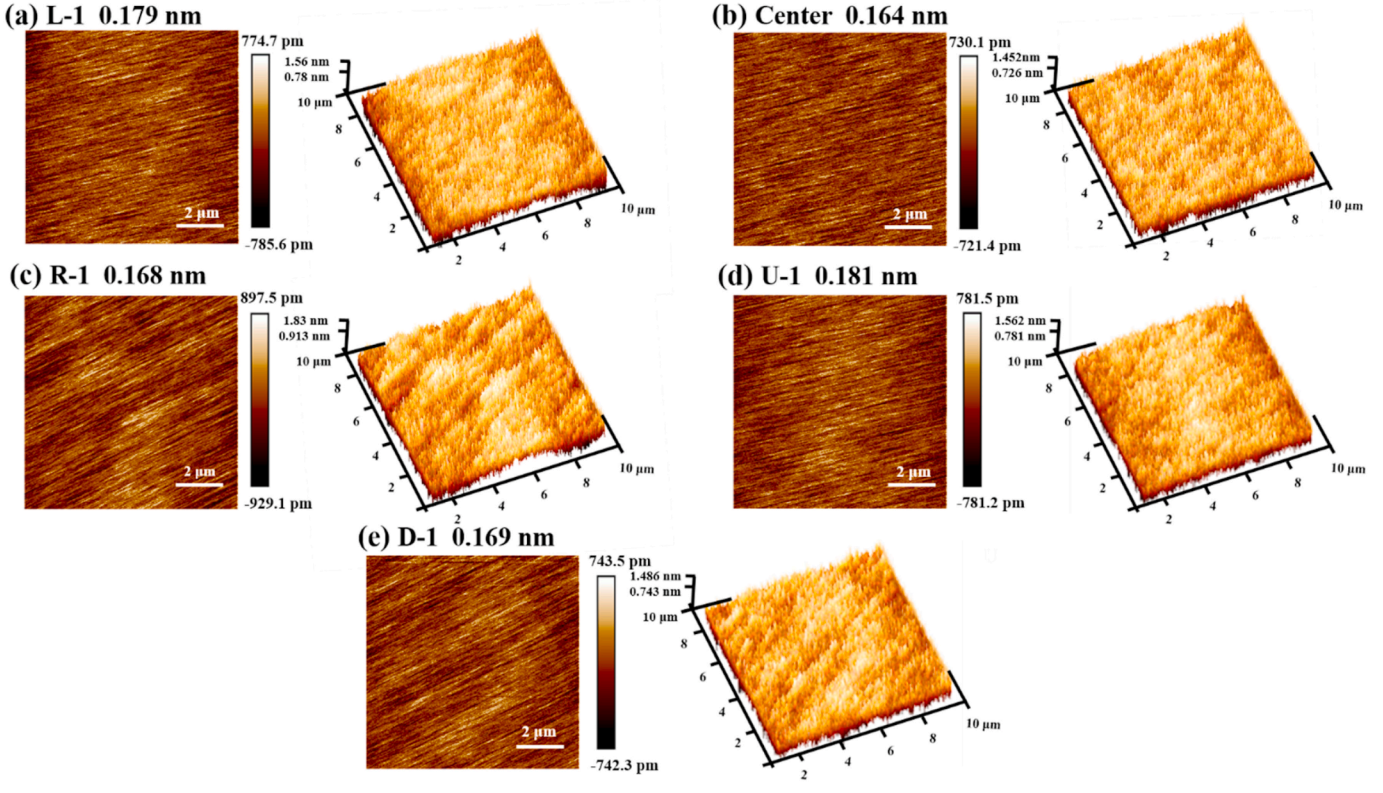

Fig. 14. Two-dimensional (2D) and three-dimensional (3D) 10 × 10 μm^2 AFM image of the epitaxial wafer at characterizing point of (a) Left-1; (b) Center; (c) Right-1; (d) Up-1; (e) Down-1.

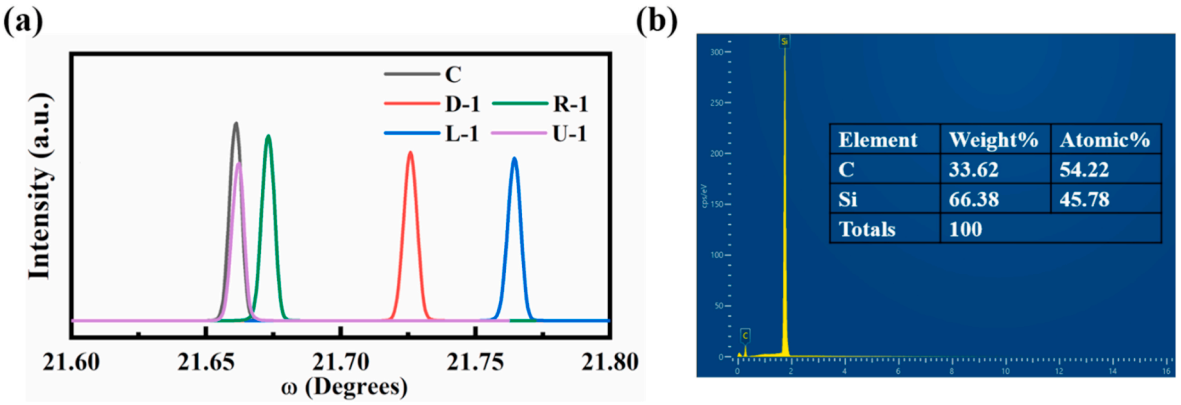

Fig. 15. (a) XRD rocking curve spectra of the 5 points on epitaxial wafer. (b) EDS pattern of epitaxial wafer.

(2) For single-factor analysis, increasing the cavity pressure and growth temperature leads to poor film quality, while enhancing the inlet-flow volume leads to superior film quality. The rotating susceptor improves the quality of the film compared with the stationary susceptor.

(3) The BPNN was adopted as a prediction model to fit the nonlinearity relationship between the combination of process parameters and film quality. The prediction results revealed that the BPNN exhibited superior performance in predicting the deposition rate and uniformity. The ant colony algorithm was introduced to search for the optimal combination of process parameters. Through ACO, the overall deposition rate increased by 17.2 % and the uniformity increased by 51.88 % compared with the standard condition. Notably, the error between the optimized after ACO-BPNN and the experiment was 4.03 % for the deposition rate and 0.49 % for the coefficient of variation. The average RMS value of surface roughness in the epitaxial wafer was 0.177 nm. Through analysis of XRD and EDS spectra, the epitaxial layer has outstanding crystallinity.

These results proved that superior film quality could be achieved from this machine learning-assisted multi-physics simulation method, which is valuable for future engineering applications in 4H–SiC epitaxial growth.

CRediT authorship contribution statement

Zhuorui Tang: Writing – original draft, Methodology, Formal analysis, Data curation. **Shibo Zhao:** Writing – review & editing, Investigation. **Jian Li:** Investigation, Data curation. **Yuanhui Zuo:** Resources, Project administration, Data curation. **Jing Tian:** Validation, Data curation. **Hongyu Tang:** Writing – review & editing, Validation. **Jiajie Fan:** Supervision, Resources. **Guoqi Zhang:** Supervision.

Declaration of competing interest

The authors declare that they have no known competing financial interests or personal relationships that could have appeared to influence the work reported in this paper.

Data availability

No data was used for the research described in the article.

Acknowledgments

This study was supported by the Science and Technology Development Plan Project of Jilin Province [Grant No. YDZJ202304QY-CX001], Shanghai Research Center for Silicon Carbide Power Devices Engineering & Technology Project [Grant No. 19DZ2253400], and the Postdoctoral Research Fund of Foshan University [Grant No. BKS217009].

Appendix A. Supplementary data

Supplementary data to this article can be found online at https://doi.org/10.1016/j.csite.2024.104507.

References

[1] S. La Mantia, V. Giuffrida, S. Buonomo, Benefits and advantages of using SiC, in: PCIM Europe 2019; International Exhibition and Conference for Power Electronics, Intelligent Motion, Renewable Energy and Energy Management, VDE, 2019, pp. 1–4.
[2] C.M. Zetterling, L. Lanni, R. Ghandi, B.G. Malm, M. Östling, Future high temperature applications for SiC integrated circuits, Phys. Status Solidi C 9 (7) (2012) 1647–1650.
[3] S. Dimitrijev, J. Han, H.A. Moghadam, A. Aminbeidokhti, Power-switching applications beyond silicon: status and future prospects of SiC and GaN devices, MRS Bull. 40 (5) (2015) 399–405.
[4] V. Jokubavicius, et al., Growth optimization and applicability of thick on-axis SiC layers using sublimation epitaxy in vacuum, J. Cryst. Growth 448 (2016)

51–57.
[5] M. Kitabatake, SiC/Si heteroepitaxial growth, Thin Solid Films 369 (1–2) (2000) 257–264.
[6] H. Pedersen, et al., Chloride-based CVD growth of silicon carbide for electronic applications, Chem. Rev. 112 (4) (2012) 2434–2453.
[7] Y. Li, et al., Reduction of morphological defects in 4H-SiC epitaxial layers, J. Cryst. Growth 506 (2019) 108–113.
[8] S. Yang, et al., Growth of 4H-SiC epitaxial layers at temperatures below 1500° C using trichlorosilane (TCS), J. Cryst. Growth 612 (2023) 127058.
[9] M. Yazdanfar, I.G. Ivanov, H. Pedersen, O. Kordina, E. Janzén, Reduction of structural defects in thick 4H-SiC epitaxial layers grown on 4° off-axis substrates, J. Appl. Phys. 113 (22) (2013).
[10] S. Leone, A. Henry, E. Janzén, S. Nishizawa, Epitaxial growth of SiC with chlorinated precursors on different off-angle substrates, J. Cryst. Growth 362 (2013) 170–173.
[11] P. Mollick, R. Venugopalan, D. Srivastava, CFD coupled kinetic modeling and simulation of hot wall vertical tubular reactor for deposition of SiC crystal from MTS, J. Cryst. Growth 475 (2017) 97–109.
[12] M. Ito, et al., Simulation study of high-speed wafer rotation effects in a vertical reactor for 4H-SiC epitaxial growth on 150 mm substrates, Mater. Sci. Forum 778 (2014) 171–174 Trans Tech Publ.
[13] S.-i. Nishizawa, M. Pons, Growth and doping modeling of SiC-CVD in a horizontal hot-wall reactor, Chem. Vap. Depos. 12 (8-9) (2006) 516–522.
[14] Y. Dang, et al., Numerical investigation of solute evaporation in crystal growth from solution: a case study of SiC growth by TSSG method, J. Cryst. Growth 579 (2022) 126448.
[15] B. Deivendran, V.M. Shinde, H. Kumar, N.E. Prasad, 3D modeling and optimization of SiC deposition from CH3SiCl3/H2 in a commercial hot wall reactor, J. Cryst. Growth 554 (2021) 125944.
[16] S. Mirjalili, S. Mirjalili, Genetic algorithm. Evolutionary Algorithms and Neural Networks: Theory and Applications, 2019, pp. 43–55.
[17] X. Yan, H. Liu, Z. Zhu, Q. Wu, Hybrid Genetic Algorithm for Engineering Design Problems, vol. 20, Cluster Computing, 2017, pp. 263–275.
[18] D. Wang, D. Tan, L. Liu, Particle swarm optimization algorithm: an overview, Soft Comput. 22 (2018) 387–408.
[19] Y.-c. Wu, J.-w. Feng, Development and application of artificial neural network, Wireless Pers. Commun. 102 (2018) 1645–1656.
[20] G. Guo, H. Wang, D. Bell, Y. Bi, K. Greer, KNN model-based approach in classification, in: On the Move to Meaningful Internet Systems 2003: CoopIS, DOA, and ODBASE: OTM Confederated International Conferences, CoopIS, DOA, and ODBASE 2003, Catania, Sicily, Italy, November 3-7, 2003. Proceedings, Springer, 2003, pp. 986–996.
[21] J. Li, J. Wang, Y. Pei, G. Wang, Research and optimization of ZnO-MOCVD process parameters using CFD and genetic algorithm, Ceram. Int. 46 (1) (2020) 685–695.
[22] J. Li, J. Wang, Y. Pei, G. Wang, Study on the uniformity of ZnO films grown by MOCVD, Ceram. Int. 45 (11) (2019) 13971–13978.
[23] J. Wang, et al., High-speed flow field prediction and process parameters optimization in a vertical MOCVD reactor based on a hybrid RSM-KNN model, Int. Commun. Heat Mass Tran. 129 (2021) 105741.
[24] Y. Tsunooka, N. Kokubo, G. Hatasa, S. Harada, M. Tagawa, T. Ujihara, High-speed prediction of computational fluid dynamics simulation in crystal growth, CrystEngComm 20 (41) (2018) 6546–6550.
[25] M. Isono, S. Harada, K. Kutsukake, T. Yokoyama, M. Tagawa, T. Ujihara, Optimization of flow distribution by topological description and machine learning in solution growth of SiC, Advanced Theory and Simulations 5 (9) (2022) 2200302.
[26] C. Cavallotti, F. Rossi, S. Ravasio, M. Masi, A kinetic analysis of the growth and doping kinetics of the SiC chemical vapor deposition process, Ind. Eng. Chem. Res. 53 (22) (2014) 9076–9087.
[27] A. Fiorucci, D. Moscatelli, M. Masi, Homoepitaxial silicon carbide deposition processes via chlorine routes, Surf. Coating. Technol. 201 (22–23) (2007) 8825–8829.
[28] A. Veneroni, F. Omarini, M. Masi, Silicon carbide growth mechanisms from SiH4, SiHCl3 and nC3H8, Cryst. Res. Technol.: Journal of Experimental and Industrial Crystallography 40 (10-11) (2005) 967–971.
[29] F. La Via, M. Camarda, A. La Magna, Mechanisms of growth and defect properties of epitaxial SiC, Appl. Phys. Rev. 1 (3) (2014).
[30] L. Zhao, Surface defects in 4H-SiC homoepitaxial layers, Nanotechnology and Precision Engineering 3 (4) (2020) 229–234.
[31] W.Y. Chen, H.C. Ho, P.F. Yang, L.C. Hsia, The relationship between surface pits density and growth parameters during the epitaxial growth of 4H-SiC, Mater. Sci. Forum 858 (2016) 229–232 Trans Tech Publ.
[32] T. Kimoto, et al., Understanding and reduction of degradation phenomena in SiC power devices, in: 2017 IEEE International Reliability Physics Symposium (IRPS), IEEE, 2017 2A-1.1-2A-1.7.
[33] S. Zhao, et al., Surface uniformity of wafer-scale 4H-SiC epitaxial layers grown under various epitaxial conditions, Coatings 12 (5) (2022) 597.
[34] A. Kamalianfar, M.G. Naseri, S.P. Jahromi, Preparation and gas-sensing performances of Cr2O3-decorated ZnO nanostructures grown in a boundary layer of non-uniform thickness for low-working temperature H2S detection, Chem. Phys. Lett. 732 (2019) 136648.
[35] Z. Shen, F. Zhang, X. Liu, G. Sun, Y. Zeng, Influence of H2 treatment on the surface morphology of SiC with different wafer orientation and doping, J. Cryst. Growth 607 (2023) 127105.